PAPER

Pseudocapacitive behaviour in sol-gel derived electrochromic titania nanostructures

To cite this article: Roberto Giannuzzi *et al* 2021 *Nanotechnology* **32** 045703

IOP Publishing Nanotechnology

Nanotechnology **32** (2021) 045703 (12pp) https://doi.org/10.1088/1361-6528/abbceb

Pseudocapacitive behaviour in sol-gel derived electrochromic titania nanostructures

Roberto Giannuzzi[1,*], Tania Prontera[1], David M Tobaldi[2], Marco Pugliese[1], Luisa De Marco[1], Sonia Carallo[1], Giuseppe Gigli[1,3], Robert C Pullar[2,4,*] and Vincenzo Maiorano[1]

[1] CNR NANOTEC—Institute of Nanotechnology, c/o campus Ecotekne, University of Salento, Via Monteroni, 73100 Lecce, Italy
[2] Department of Materials and Ceramics Engineering and CICECO−Aveiro Institute of Materials—University of Aveiro, 3810–193 Campus Universitário de Santiago, Portugal
[3] Dipartimento di Matematica e Fisica E. de Giorgi, Università Del Salento, Campus Ecotekne, via Monteroni, Lecce, 73100, Italy
[4] Department of Molecular Sciences and Nanosystems, Ca' Foscari University of Venice, Scientific Campus, Via Torino 155, 30172 Mestre (VE), Italy

E-mail: roberto.giannuzzi@nanotec.cnr.it and rpullar@ua.pt

Received 29 June 2020, revised 23 September 2020
Accepted for publication 30 September 2020
Published 26 October 2020

Abstract

Nanostructured thin films are widely investigated for application in multifunctional devices thanks to their peculiar optoelectronic properties. In this work anatase TiO_2 nanoparticles (average diameter 10 nm) synthesised by a green aqueous sol-gel route are exploited to fabricate optically active electrodes for pseudocapacitive-electrochromic devices. In our approach, highly transparent and homogeneous thin films having a good electronic coupling between nanoparticles are prepared. These electrodes present a spongy-like nanostructure in which the dimension of native nanoparticles is preserved, resulting in a huge surface area. Cyclic voltammetry studies reveal that there are significant contributions to the total stored charge from both intercalation capacitance and pseudocapacitance, with a remarkable 50% of the total charge deriving from this second effect. Fast and reversible colouration occurs, with an optical modulation of ~60% in the range of 315–1660 nm, and a colouration efficiency of 25.1 $cm^2\ C^{-1}$ at 550 nm. This combination of pseudocapacitance and electrochromism makes the sol-gel derived titania thin films promising candidates for multifunctional 'smart windows'.

Supplementary material for this article is available online

Keywords: TiO_2, electrochromics, pseudocapacitance, sol-gel

(Some figures may appear in colour only in the online journal)

1. Introduction

Titanium dioxide (TiO_2) is one of the most widely used transition-metal oxides due to its high mechanical and chemical stability, cost-effectiveness, as well as for its non-toxicity and abundance [1]. TiO_2 films are extensively studied for applications in photocatalysis, solar cells, rechargeable batteries, gas sensors, and electrochromic (EC) devices [2–8].

EC devices are characterised by a reversible and persistent change of the optical properties by means of a redox reaction or by application of a proper electrochemical potential [9]. The optical effect is due to reversible injection or extraction of ions (such as H^+, Li^+, Na^+) and simultaneous electrons (e^-) balancing charge in the active material.

* Authors to whom any correspondence should be addressed.

WO_3, Nb_2O_5 and TiO_2 are among the most used active inorganic materials for applications in EC cells [10]. Specifically, TiO_2 is a good candidate for EC applications, thanks to its wide band-gap (3.2 eV for anatse, 3.0 eV for rutile) and suitable crystal lattice structure that confers good transparency of the thin films and easy field-aided ion intercalation. The Li^+ ion intercalation or insertion process is accompanied by a reduction process, as some of the Ti^{4+} is reduced to Ti^{3+} to compensate for the Li^+, leading to a colour change of the material (cathodic colouration, typically darkening). This is because there is a change of visible light absorption, ascribed to the generation of polaron states [11–13].

Different methods have been used for the production of TiO_2 as cathodic EC material, such as reactive radio frequency and direct current magnetron sputtering [14], chemical solution deposition [15], dipping sol-gel [16], reactive electron beam evaporation [17], and atmospheric pressure chemical vapour deposition [18]. The results reported for different production processes demonstrate that the deposition methods and conditions strongly affect the electrochemical properties of thin films.

In fact, in addition to their electrochromic properties, these semiconductors also can show charge storage capability that can be exploited in batteries. In particular, a rate dependent charge/discharge mechanism is observed with the reduction of the TiO_2 particle dimensions [19]. Indeed, diffusion-controlled lithium ion intercalation process (which is at the basis of the EC function) is observed for bulk materials but a faradic process involving surface or near surface redox reaction (on which relies the storage capability) appears when approaching the nanoscale regime.

This faradic-based charge storage phenomenon is recognised as pseudocapacitance, and the related materials are known as 'pseudocapacitive materials'.

Differently from 'intrinsic psudocapacitive' (such as RuO_2 and MnO_2) [20, 21], TiO_2 [19] can be considered an 'extrinsic pseudocapacitive' material since this behaviour is a consequence of the particle size reduction. TiO_2 is of great interest since it has been proven to be a promising candidate for both Li-ion [19, 22, 23] and Na-ion [24–26] pseudocapacitance and, in addition, is a very promising pseudocapacitive material in acidic electrolytes. Therefore, pseudocapacitive materials with additional EC properties can be easily obtained by designing nanoscale metal oxides that combine good charge storage and fast kinetics, opening new opportunities for the production of multifunctional devices like smart windows or dynamic shading elements [27–29]. Further investigations are mandatory to better understand the different pseudocapacitance behaviours, in order to improve the performance of these 'EC supercapacitors' for practical applications.

In this study, we investigate the pseudocapacitive behaviour and electrochromic properties of nanostructured films consisting of TiO_2 nanoparticles with sizes ~10 nm synthesised via a simple, green and aqueous sol-gel process. In order to understand the potential of the obtained results, the newly synthesised materials were compared with those of commercial TiO_2 nanoparticles. We developed a method to prepare electrodes without the inclusion of conductive components. The use of engineered nanostructures allows the transition from a purely diffusion controlled charge-storage process, due to Li^+ intercalation into the TiO_2 lattice, to a mixed diffusion- and capacitance-controlled charge-storage process, associated with Li^+ adsorption on the TiO_2 surface. The resulting highly transparent and very thin films (100 nm thick) showed a pseudocapacitive behaviour responsible for about 50% of the total capacitance under tested potential. This leads to overall charging/discharging rates that are much faster for the smaller nanoparticles compared to the larger commercial nanoparticles. An optical modulation of ~60% was obtained in the visible and near-infrared wavelength range (315–1660 nm) between the bleached and the coloured state, and a coloration efficiency (CE) of 25.1 $cm^2\,C^{-1}$ at 550 nm. The pseudocapacitive beahviour alleviates the stress resulting from multiple intercalation/deintercalation lithium ion cycles, resulting in long-term stability of the electrode. Thus, TiO_2 nanoparticles display promise as a bifunctional material combining electrochromic and pseudocapacitive properties, showing tremendous application potential for use in energy-storing smart windows.

2. Experimental

2.1. Sample preparation

2.1.1. Synthesis of sol-gel titania films. The synthesis of these aqueous sols is based on our previously published syntheses for pure [30, 31] titania sols and NPs. Briefly, 0.2 moles of titanium-iso-propoxide (Merck, 97%) was added to 400 ml of iso-propanol and stirred at 800 RPM. 5.6 ml of concentrated HNO_3 (Fluka Puriss PA, 65 wt%) in 20 ml distilled water were added to 50 ml IPA, and this was then added dropwise to the titanium-iso-propoxide with stirring. This showed no initial precipitation, but after approximately half of the acidic solution was added a thick white precipitate formed, and the stirring rate had to be increased to ~1200 RPM. After about ¾ of the acidic solution had been added, the precipitate became less viscous, resembling milk, and stirring could be reduced to 800 RPM again. Total addition time was about 30 min. This mixture was then placed on a rotary evaporator and the solvent removed at 60 °C, 100 mbar pressure, to produce a thick white gel which resembles coconut cream in consistency. This was redispersed in 400 ml of distilled water, and then the water removed by rotary evaporator at 60 °C, 70 mbar pressure to produce a viscous but powdery yellow gel which never fully dried. Another 400 ml of distilled water was added, the gel redispersed, and the water removed at 60 °C, 70 mbar pressure until a viscous yellow gel had formed. Distilled water was added to make a total volume of 200 ml, and the gel redispersed to create a yellowish-white sol, 1 M concentration.

Unlike in our previous syntheses, 5 wt% PAA ($–CH_2CHCO(OH)–$, Aldrich PAA Nº 323667, Av. MW = 1800) was added to this sol as a surfactant, to stablise the sol during the coating process and produce transparent

films. 5 wt% PAA (5 wt% to TiO_2) was dissolved in water and added to the sol. The sol appeared slightly more viscous and was a paler white after PAA addition.

2.1.2. Film preparation. To obtain the nanostructured thin films, the TiO_2-PAA sol (5 ml) was stirred at room temperature for 30 min, and a solution of 0.05 g of the binder ethylcellulose (30–70 mPa s, provided by Sigma Aldrich) previously dissolved in methanol (10% wt/wt); fluorine-doped tin oxide (FTO, 15 Ω sq^{-1}, provided by Kintec) glass plates were first cleaned in a detergent solution using an ultrasonic bath for 15 min, and then rinsed with water and ethanol, and used as substrates. The NP—binder solutions were spin coated on 1 cm^2 FTO substrates at 1500 rpm/30 s, and annealed at 430 °C/30 min in air. All samples were highly transparent and homogeneous. Films were also made with suspensions of Evonik/Degussa P25 and Dyesol 18NRT as follows.

Evonik/Degussa P25-based paste was prepared according the reported literature [32, 33]. Briefly, TiO_2 powder was grinded in a porcelain mortar with acetic acid, water and ethanol. This TiO_2 dispersion was transferred from mortar to a beaker with excess of ethanol and then stirred and sonicated. Anhydrous terpineol and ethyl cellulose in ethanol were added, followed by stirring and sonication. The P25 suspension was deposited by spin coating and annealed as above indicated. Commercial screen-printable paste, Dyesol 18NRT, was diluted with ethanol, stirred for 2 h at 50 °C and deposited with the same process used for NP TiO_2 and P25.

2.2. Sample characterisation

2.2.1. Structural and morphological characterisation. Low-resolution TEM investigation of scratched flakes of nanostructured RP-TiO2 thin film was performed with a JEM 1400Plus microscope, operating at an acceleration voltage of 120 kV.

The nanostructured film thickness was measured using a Veeco Dektak 150+ Profiler.

Atomic force microscopy (AFM) image was recorded by a Park XE-100 model in no-contact mode.

2.2.2. Electrochemical and spectro-electrochemical characterisation. Electrochemical and spectroelectrochemical measurements of the films were carried out in a three electrode configuration with a platinum foil as the counter electrode (area 4 cm^2) and an Ag/AgCl electrode in 1 M $LiClO_4$ in propylene carbonate as the reference electrode. The electrolyte solution was anhydrous 1 M $LiClO_4$ in propylene carbonate. The active area of the film (working electrode) was 1 cm × 1 cm. All measurements were carried out within the electrochemical stability window of the electrolyte (−1.5/+0.1 V) determined with cyclic voltammetry (CV). *In situ* optical spectra were recorded at several potentials after allowing for stabilisation of the optical signal, which required several minutes. The path length of the electrolyte was <5 mm during the measurements [34]. Charge measurements between the potential limits were performed via chronoamperometry, with a potential switched between −1.5 and +0.1 V for a 60 s holding time. Colouration efficiency (CE) was calculated from the slope of the optical density (OD) as a function of the charge density. All electrochemical measurements were performed with an AUTOLAB PGSTAT302N potentiostat and a Varian Cary 5000 UV−VIS−NIR spectrophotometer.

3. Result and discussion

3.1. Structural and morphological analysis on TiO_2 sample

TiO_2 nanoparticles (NPs) synthesised by an aqueous sol-gel process (see experimental section for further details and figure S1 is available online at stacks.iop.org/NANO/32/045703/mmedia for a flow-chart describing the preparation procedure) have been fully characterised, and their physical and crystallographic properties discussed previously [30, 31]. To summarise, when calcined at 450 °C/2 h the pure TiO_2 NPs consisted of 25.1 wt% anatase, 37.7 wt% rutile, 10.3 wt% brookite and 26.9 wt% amorphous phases. The calculated diameters of crystalline domains were 9.9 nm for anatase, 14.1 nm for rutile and 3.2 nm for brookite, although the actual particle size ranged from 10 nm up to 50 nm and they were heavily prone to clustering [31]. Previous studies have shown that P25 consists of 76.3 wt% anatase, 10.6 wt% rutile and 13.0 wt% amorphous phases [35] while Dyesol 18NRT titania paste is claimed by the manufacturers to be 99% anatase [36].

When spin coated onto the FTO-glass substrates, pure calcined sol-gel TiO_2 nanoparticles gave opaque films due to clustering of the NPs, and hence were not suitable for electrochromic devices. Therefore, 5 wt% of polyacrylic acid (PAA) surfactant was added to the sols in order to prevent NP coalescence during the deposition and the subsequent sintering process. PAA was then burnt out with annealing at 430 °C, leaving a very even, transparent TiO_2 nanostructured film, probably with increased porosity due to the loss of the PAA. Figure S2 shows digital images of the TiO_2 films after annealing process.

SEM and TEM images of the as-produced nanostructured films, henceforth named RP-TiO_2, are shown in figures 1(a) and (b), respectively. As can be seen in figure 1(a), TiO_2 films presented a smooth surface, characterised by a good spatial homogeneity and the absence of clusters. As expected, nanoparticles and mesopores were below the resolution of the SEM instrument (i.e. <30 nm), suggesting that the original NP size has been adequately retained. This was confirmed by the TEM analysis carried out on scratched portions of the electrode: it can be seen that the building blocks of the thin film are NPs sized around 10 nm, partially fused to each other at the edges.

For comparison we prepared two other thin films based on commercially available nanotitania, namely P25 Degussa (P25-TiO_2) and Dyesol 18NRT colloidal paste (Dyesol-TiO_2). The SEM images clearly show a coarser morphology than the RP-TiO_2 film, despite the manufacturers claiming similar particle sizes of around 20 nm. Dyesol-TiO_2

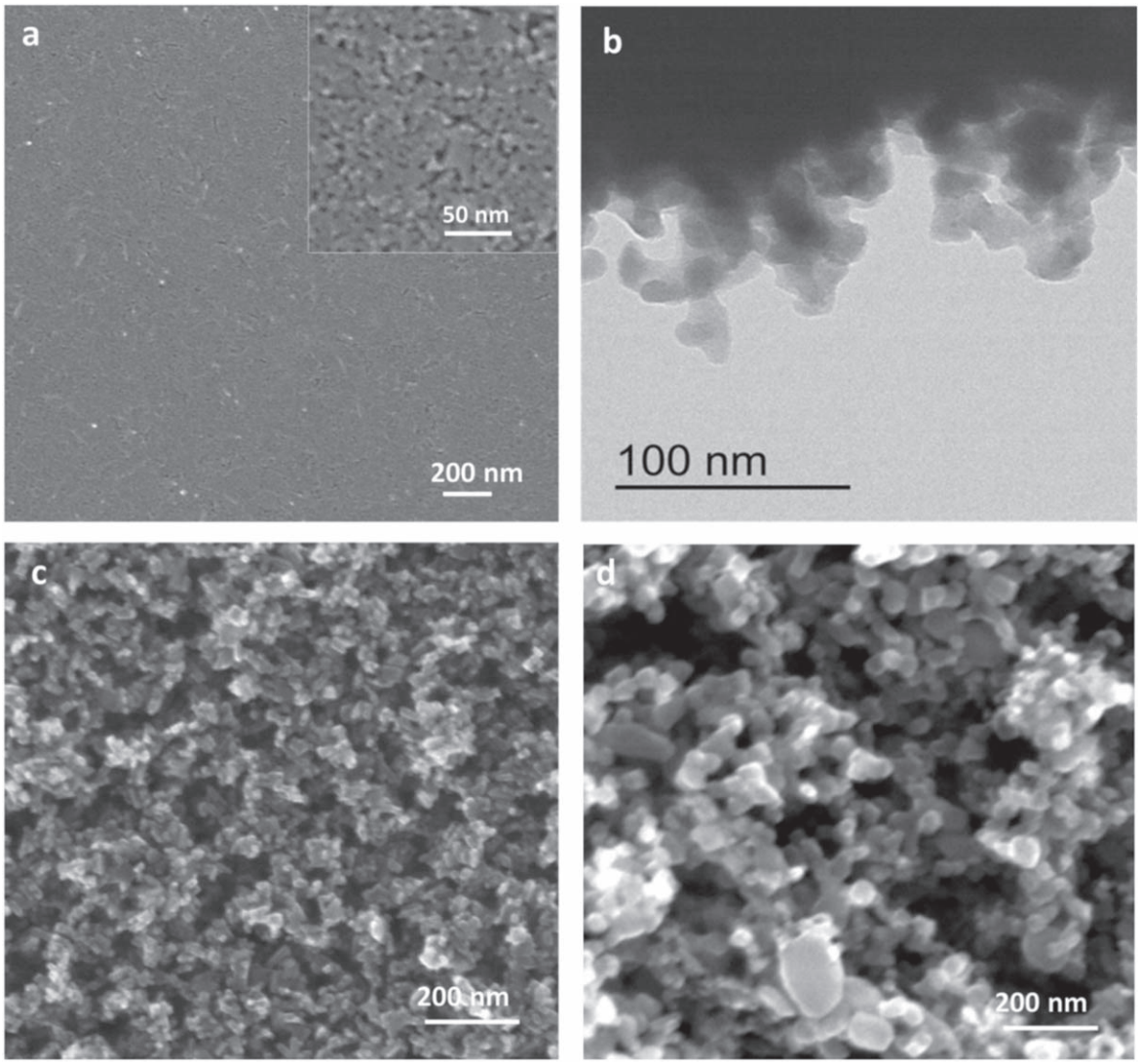

Figure 1. (a) and (b) SEM and TEM images of RP-TiO_2 thin films, respectively. (c) and (d) SEM images of Dyesol-TiO_2 and P25-TiO_2 thin films, respectively.

and P25-TiO_2 are made up of nanoparticles sized 50 nm and 100–200 nm, respectively, suggesting that these electrodes should have less surface area.

The morphology of the thin films was also investigated by AFM, reported in figure S3, which showed a very compact layer for RP-TiO_2 with a root-mean-square (rms) roughness of ∼4.2 nm and rougher surface topographies for the commercial TiO_2, with a rms of ∼17 nm and ∼115 nm for Dyesol-TiO_2 and P25-TiO_2, respectively.

3.2. Pseudocapacitive behaviour analysis on TiO_2 samples

The electrochemical performance of RP-TiO_2, P25-TiO_2 and Dyesol-TiO_2 were tested with CV technique at different scan rates ranging from 1 to 20 mV s^{-1} in 1 M $LiClO_4$ based electrolyte. The first four CV scans at 1 mV s^{-1} are reported in figures 2(a)–(c). The voltammogram shape and current values are stable after 3 cycles, as evidence of the good electrochemical stability of the electrodes under investigation. A small reduction of the area under the curve occurs, and it is about 8% of the initial value. This small capacitance loss is usually attributed to irreversible phase changes, ion trapping at the defect sites of TiO_2 nanoparticles, or an irreversible reaction of Li^+ with adsorbed water molecules [37–39]. All samples show a cathodic peak around −1.3 V and an anodic peak around −1.0 V. These reported CV peaks are typical for anatase-based electrodes, and they are attributable to the intercalation/deintercalation processes of lithium ions into the anatase structure:

$$TiO_2 + xLi^+ + xe^- \leftrightarrow Li_xTiO_2,$$

where x is the insertion coefficient usually close to 0.5.

The large peak separation between the cathodic and anodic peaks indicates the irreversibility of the electrochemical process. The shift of the peak with the change of the scan rate (figure S4) further confirms that the investigated process is electrochemically irreversible. Specifically, the peak separation for RP-TiO_2 is 0.37 V, and is smaller than that of TiO_2-Dyesol (0.42 V) and TiO_2-P25 (0.48 V). The higher peak-peak potential separation for the commercially

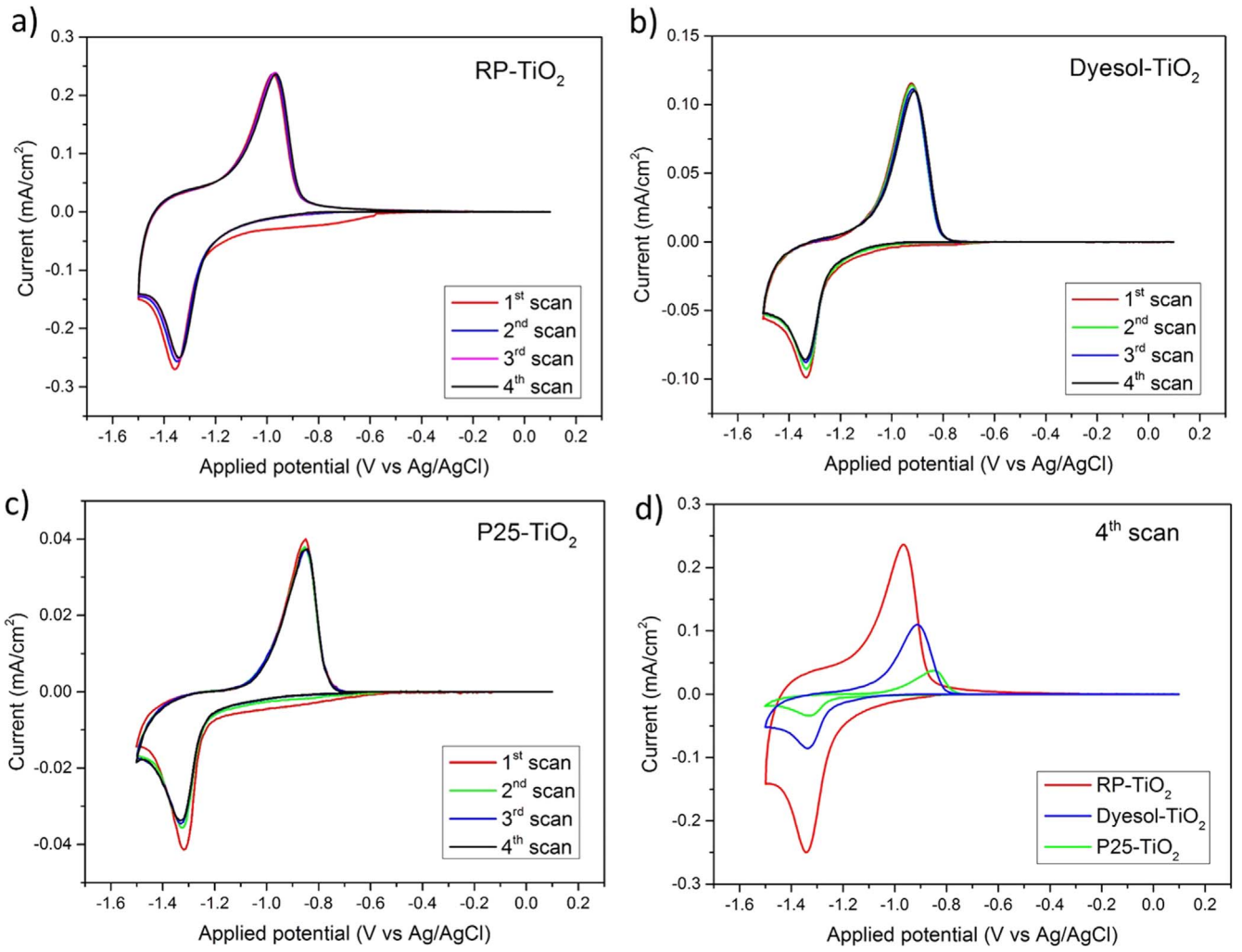

Figure 2. Cyclic voltammogramms for (a) RP-TiO_2, (b) Dyesol-TiO_2 and (c) P25-TiO_2 electrode recorded at a scan rate of 1 mV s^{-1}. (d) Fourth cycle of the each set of voltammetry recorded at 1 mV s^{-1}.

available TiO_2 film can be attributed to slower ion intercalation/deintercalation kinetics. In TiO_2 films, peak separation is determined by the overpotential required to transform TiO_2 into Li_XTiO_2, and it is largely demonstrated that such overpotential is smaller when the surface area is higher [40, 41]. Indeed, less peak separation observed in RP-TiO_2 electrodes should be related to their finer morphology (larger surface area) with respect to reference electrodes, in accordance with the SEM images reported in figure 1. In figure 2(d), the voltammogram of the three TiO_2 electrodes at 1 mV s^{-1} are reported. The higher charge storage capacity of RP-TiO_2 is clearly visible by considering the greater area under the peaks. The quantity of stored charge, obtained by integrating the area under the cathodic peak, is 50 mC cm^{-2} for RP-TiO_2, 15 mC cm^{-2} for Dyesol-TiO_2 and finally 5 mC cm^{-2} for P25-TiO_2. The total stored charge was normalised with the geometric area (about 1 cm^2) since the sample preparation preclude the direct measurement of the mass.

Keeping in mind that as all the samples had the same thickness and geometric area, the higher amount of stored charge in RP-TiO_2 can be ascribed to higher surface area due to the smaller particle size of the starting material.

The charge storage properties were investigated by analysing the cyclic voltammetry data at various sweep rates according to the following relation:

$$i = av^b, \tag{1}$$

where both a and b are adjustable parameters and v is the sweep rate [19, 42]. The b values are determined from the slope of the linear plot of log I versus log v. A b value close to 1 corresponds to a capacitive regime in which the fast surface redox reactions and the double layer charging are the most relevant processes, while a b value of 0.5 is typical of bulk diffusion-controlled faradic processes. From the analysis of the CV data, at the peak potential of −1.3 V, the b value of RP-TiO_2 is 0.67, while b is in the range of 0.8–1.0 for potential values higher and lower than −1.3 V. The reported b values indicate that at −1.3 V the Li ion intercalation reaction is predominant, whereas a capacitive mechanism prevails at higher and lower potentials. The reference samples show the same b-value trends, but with lower values due to smaller pseudocapacitance contribution. The correlation between the

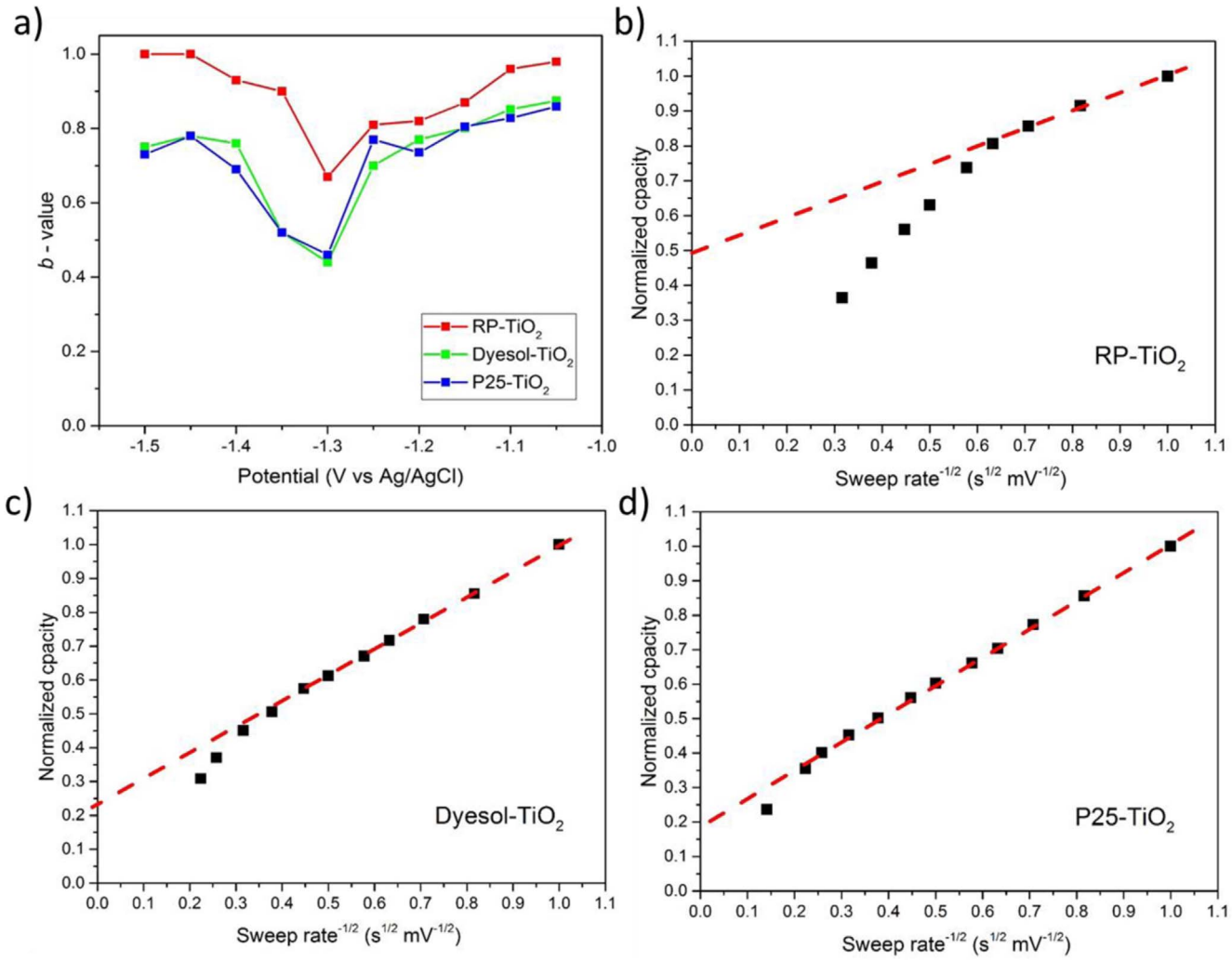

Figure 3. (a) *b*-values for the TiO_2 nm film plotted as a function of potential for cathodic sweeps (Li^+ insertion). Normalised capacity versus $v^{-1/2}$ for (b) RP-TiO_2, (c) Dyesol-TiO_2 and (d) P25-TiO_2. The dashed red line corresponds to the extrapolation of the infinite sweep rate capacitance using the capacity between 1 and 20 mV s^{-1}.

capacitance and the sweep rate can be used to identify the rate-limiting step of the charge-storage process.

Trasatti's analysis was applied to gain further insight with respect to the kinetics of charge [43]. This analysis describes the relationship between the capacity and the sweep rate. Capacity that is occurring due to surface processes will be constant with the sweep rate, and thus will always be present, even at high sweep rates. Capacity that occurs due to diffusion-controlled processes will vary with $v^{-1/2}$. In the following equation, the capacitive contribution is represented by $Q_{v=\infty}$, which is the infinite-sweep rate capacity; the diffusion-controlled capacity is the remaining contribution, and is limited by $v^{-1/2}$

$$Q = Q_{v=\infty} + \text{constant}(v^{-1/2}).$$

In the plot of normalised capacity versus $v^{-1/2}$, (figures 3(b)–(d)), the extrapolation of the linear fit to the data to the *y*-intercept ($v^{-1/2} = 0$) gives $Q_{v=\infty}$. As shown in figures 3(b)–(c), the relative ratio of $Q_{v=\infty}$ gradually increases with increasing sweep rate, and it is 50% for RP-TiO_2 at 1 mV s^{-1}, which represents the contribution of the so-called outer surface of RP-TiO_2 to the charge storage. The same analysis performed on Dyesol-TiO_2 and P25-TiO_2 revealed values of $Q_{v=\infty}$ of 23% and 18%, respectively. Clearly, the capacitive contributions from the smaller particles are significantly higher than those from the larger particles. The synthesised nanoparticles possess small size and high surface area to volume ratio, which promotes the high-rate capability, due to the increase in the surface lithium-ion storage sites, and the decrease in the diffusion length of lithium ions during the insertion/extraction process [44, 45]. Moreover, extrinsic pseudocapacitance emerges when the synthesised nanoparticles are processed as thin film so that a large percentage of ion storage sites are dominant on the surface [46, 47]. It is well known that the pseudocapacitive performance of an electrode is directly related on the mass-loading active materials, as discussed by Gogotsi *et al* [48]. Indeed, with extrinsic pseudocapacitive materials, decreasing the thickness of the film leads to improved high-rate behaviour due to a decrease in diffusion distances and, in some cases, the suppression of a phase transformation. These two factors are well exhibited by RP-TiO_2 films making this material suitable for

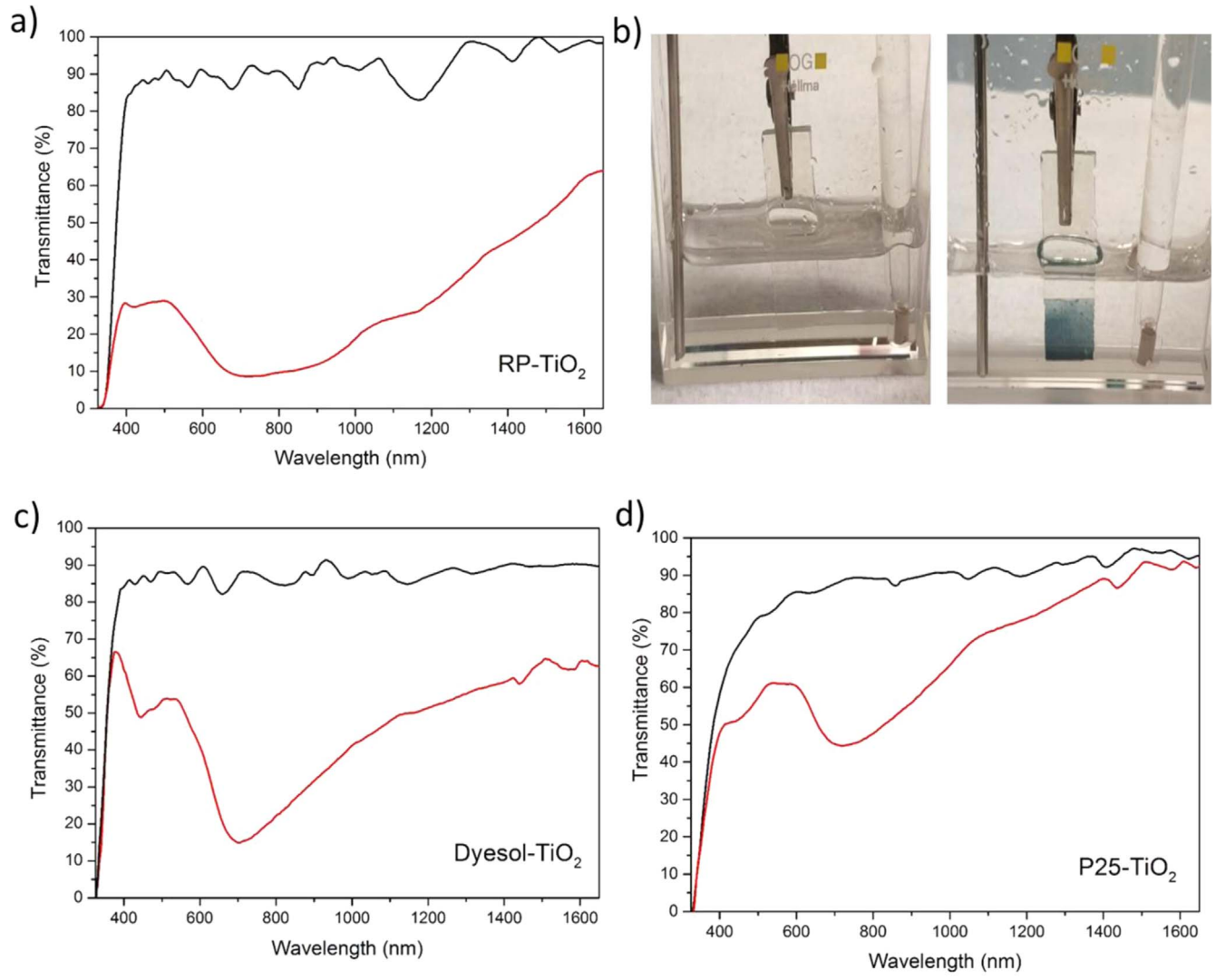

Figure 4. Transmittance spectra of the TiO_2 based electrode (thickness ≈ 100 nm) at bleached state (black curve) and coloured state (red curve) different applied bias voltages. (a) RP-TiO_2, (c) Dyesol-TiO_2 and (d) P25-TiO_2. Panel (b) shows daylight digital pictures of a RP-TiO_2 electrode in the bleached (left) and colored (right) states upon the application of −1.5 V.

multifunctional devices such as pseudocapacitive electrochromic glass windows.

3.3. Spectroelectrochemical behaviour analysis on TiO_2 samples

The transmittance spectra for 100 nm thick TiO_2 electrodes were measured *in-situ*, within the same three-electrode set-up (see figure S5), by applying a bias of 0.1 and −1.5 V (figure 4). In the bleached state, the transmittance was slightly higher for RP-TiO_2 than for Dyesol-TiO_2 and P25-TiO_2 films in the visible and NIR regions. A transmittance reduction of the TiO_2 electrodes is visible with the reduction of the applied voltage, with a linear dependence over the entire investigated wavelength range. The best result is observed for RP-TiO_2, with an overall reduction transmittance in the 350–1650 nm range higher than 60%, while Dyesol-TiO_2 and P25-TiO_2 show a reduction of 39% and 17%, respectively. In particular, RP-TiO_2 electrode turns dark bluish in the coloured state (figure 4(b)), and it is able to completely shield visible radiation and modestly reduce the transmittance in the NIR region.

To further investigate the EC properties of the TiO_2 samples, chronoamperometric measurements were carried out by applying a square wave voltage of +0.1/−1.5 V for 120 s, and by measuring the corresponding transmittance value at 550 nm (figure 5). Commonly used parameters to evaluate the kinetic of the coloration/bleaching processes are $\tau c_{/90\%}$ and $\tau b_{/90\%}$, those are the times required to reach a 90% change across the full transmittance modulation range. The faster kinetic for the coloration process is observed for RP-TiO_2 which shows a $\tau c_{/90\%}$ of 54 s, compared to 72 s and 81 s for Dyesol-TiO_2 and P25-TiO_2, respectively, and it is related to the better pseudocapacitive properties. At the same time, the bleaching kinetic is comparable for the three samples with $\tau b_{/90\%}$ values of 11, 4 and 7 s, respectively, for RP-TiO_2, Dyesol-TiO_2 and P25-TiO_2. Such kinetic results are quite interesting, since the quantity of inserted/extracted lithium ion in RP-TiO_2 is more than three times higher than that of

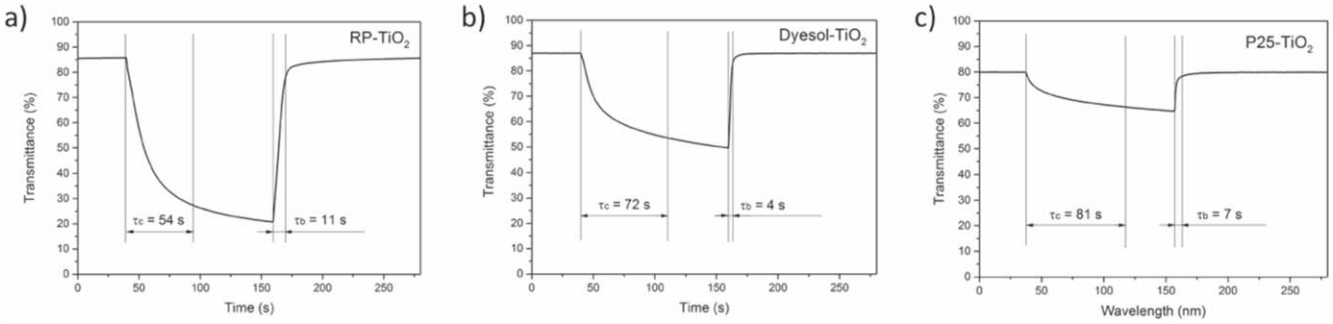

Figure 5. *In situ* transmittance variation curve monitored at the wavelengths of 550 nm, obtained by applying a square wave voltage of +0.1 V/−1.5 V for 120 s. (a) RP-TiO_2, (b) Dyesol-TiO_2 and (c) P25-TiO_2.

Table 1. Charge-storage properties and EC features of TiO_2-based electrodes measured in 1 M $LiClO_4$ in propylene carbonate using a three-electrode setup.

	$Q_{v=\infty}$ [mC cm^{-2}]	ΔT at $\lambda = 550$ nm [%]	ΔT at $\lambda = 315$–1660 nm [%]	$\tau_{c/90\%}$ [s]	$\tau_{b/90\%}$ [s]	CE [cm^2 C^{-1}]
RP-TiO_2	50	63	60	54	11	25.1
Dyesol-TiO_2	15	34	39	72	4	18.4
P25-TiO_2	5	20	17	81	7	14.8

Geometric area = 1 cm^2; thickness = 100 nm.

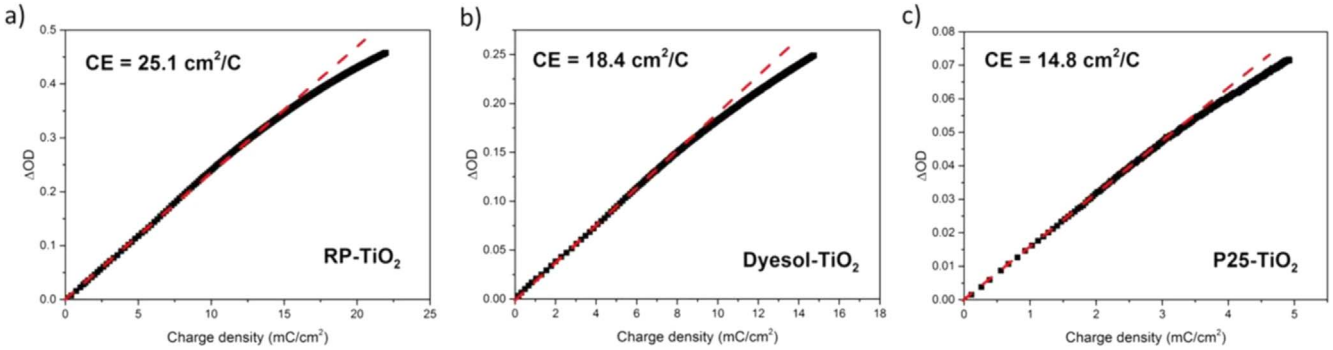

Figure 6. Plot of optical density variation as a function of charge density monitored at 550 nm. (a) RP-TiO_2, (b) Dyesol-TiO_2 and (c) P25-TiO_2.

Dyesol-TiO_2 and ten times than that of P25-TiO_2, yet the colouration process is quicker. These superior properties make RP-TiO_2 a good candidate for electrochromic devices able to efficiently and fast modulate transmittance over the visible-NIR range.

However, a substantial difference between the colouring and bleaching kinetics is observed in all investigated samples, and it is related with an asymmetry between the intercalation and de-intercalation processes. Intercalation in anatase-based titanium dioxide occurs mainly at the electrode surface, and it can be defined as a 'top-down' filling mechanism, in which the lithium intercalation leads to a build-up of Li_xTiO_2 at the electrode/electrolyte interface, which further slows down the diffusion process [40]. Vice versa, in the de-intercalation process, lithium ions at the top of the electrode are easily released into the electrolyte thus facilitating the diffusion of lithium ions from the 'bottom' of the electrode to the electrolyte. Therefore, the kinetics of the colouring process is more limited by the lithium ion diffusion compared to the bleaching phase, and this explains the higher $\tau c_{/90\%}$ values for the TiO_2 samples (table 1).

CE is another fundamental parameter for the classification of the EC materials. CE is defined as the ratio between the change of OD per unit of inserted charge:

$$CE = \Delta OD/\Delta Q = \log(Tb/Tc)/\Delta Q,$$

where ΔQ is the inserted charge, and Tb and Tc refer to the transmittance values in bleached and coloured state, respectively, at a given wavelength. High CE corresponds to a large optical modulation per amount of charge inserted/extracted, which can be regarded as an advantage in terms of time responsivity of the device and long-term stability on cycling. Calculation of the CE parameter from the slope of the linear region of the OD versus current density plot, yielded values of 25.1 $cm^2\,C^{-1}$ for RP-TiO_2, CE = 18.4 $cm^2\,C^{-1}$ for Dyesol-TiO_2 and 14.8 $cm^2\,C^{-1}$ for P25-TiO_2 at $\lambda = 550$ nm (figure 6).

Detailed data for each film at different wavelengths are reported in table 1. The better CE at NIR frequencies suggests

Table 2. Comparison of our work with previously published papers.

TiO_2 thin film preparation method	Crystalline phase				Thickness [nm]	CE [cm^2 C^{-1}]	ΔT [%]	References
	Am	A	R	B				
RP Method	X	X	X	X	100	25.1 at 550 nm	63 at 550 nm	Our work
Dyesol 18 NRT		X			100	18.4 at 550 nm	34 at 550 nm	Our work
Degussa P25	X	X	X		100	14.8 at 550 nm	20 at 550 nm	Our work
Nebulised spray pyrolysis		X			800	31.12 at 600 nm	32 at 600 nm	[49]
Dipping sol-gel		X			230		50 at 600 nm	[50]
Sol gel		X	X		280		40 at 550	[51]
Sol-gel		X	X		200	11.4 at 550 nm	49.5 at 550 nm	[52]
Doctor blade		X			600	33.7 at 550 nm	68 at 550 nm	[53]
Hydrothermal treatment of sputtered Ti		X			350	13.87 at 600 nm	28 at 600 nm	[54]
Composite TiO_2 NWs and TiO_2 NPs obtained by autoclaves + spin coating		X	X		380	17.56 at 800 nm	32 at 800 nm	[55]
Thermionic vacuum arc method		X	X		110	18.6 at 550 nm	8 at 550 nm	[56]
Linear accelerated e-beam evaporation technique (LAeB)					120	29 at 516 nm	11 at 516 nm	[57]
Metal–organic chemical vapour deposition (MOCVD)		X			240		60 at 550 nm	[58]
Anodization		X			3100	15.58 at 600 nm	70 at 600 nm	[59]
DC magnetron sputtering	X				300		50 at 550 nm	[60]

Am: Amorphous; A: Anatase; R: Rutile; B: Brookite.

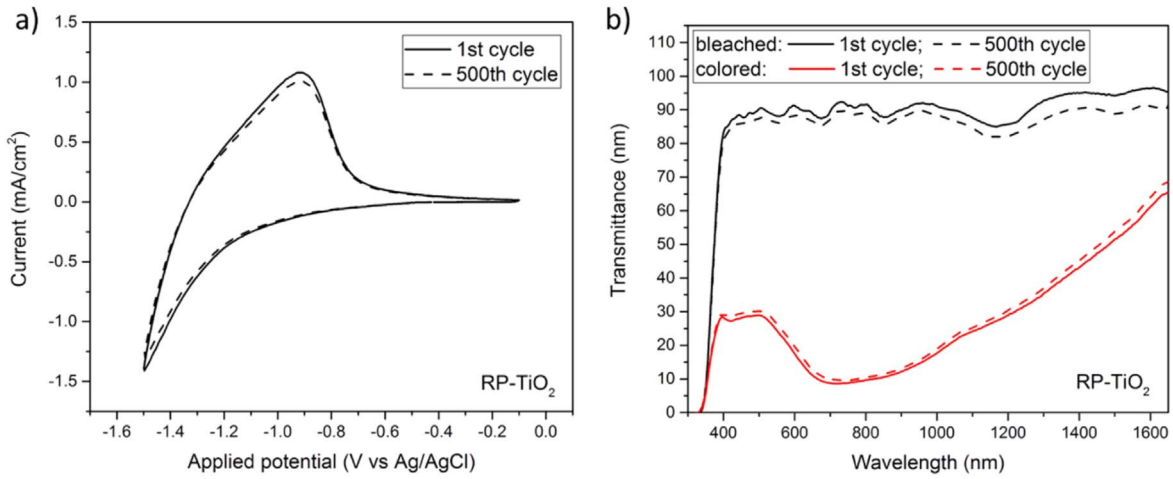

Figure 7. Cyclic voltammograms (a) and transmittance spectra of the bleached and colored state (b) for RP-TiO_2 evaluated at first cicle (straight line) and after 500 cycles at 20 mV s^{-1} (dashed line).

a more efficient EC response for RP-TiO_2 with respect to the commercial counterparts, and reflects its consistently higher surface capacitance.

Table 2 examines the results obtained with TiO_2 thin films having different crystalline phases, deposition methods and thicknesses. Our RP-TiO_2 film has a very good ΔT in absolute terms and, considering the low thickness of these films (only 100 nm), our material undoubtedly shows the best electrochromic properties among similar TiO_2 thin films previously reported. The analysis of the data shown that the presence of several crystalline phases does not have a significant impact on electrochromic properties. Therefore, it seems that the different performances are related to the nanostructure of the films. Indeed, the use of engineered nanostructures allows the emergence of a capacity-controlled charge storage process, which leads to an improvement of the electrochromic properties of our film. The reported results demonstrate that RP-TiO_2 is an interesting candidate for multifunctional EC devices thanks to its good characteristics in terms of optical contrast and coloration efficiency and the occurrence of the pseudocapacitive effect.

Finally, the cycling stability of RP-TiO_2 electrode was evaluated by carrying out continuous CV cycles at a scan rate of 20 mV s^{-1} and by measuring the corresponding transmittance spectra. As shown in figure 7(a), CV curves remain almost unchanged within 500 cycles indicating excellent cycling stability of the nanoparticle film. This result could be correlated to the beneficial role of pseudocapacitive behaviour that reduces the stress associated with Li^+ insertion/extraction. The transmittance spectra in bleached and coloured state (figure 7(b)) result almost unchanged in the visible region of the spectrum and slightly reduced in the IR region. This result is probably related to lithium ion irreversibly trapped inside the TiO_2 crystal structures that increase the absorbtion in the IR region according to the Drude model.

4. Conclusion

We have reported on the exploitation of mesoporous TiO_2 films prepared from an aqueous sol-gel process (RP-TiO_2), for the fabrication of EC and storage multifunctional active films. Detailed electrochemical and spectroelectrochemical measurements allowed us to elucidate the connection between the EC response and the morphological features of the active coating. Two competitive processes determined the charging/discharging processes at the electrodes: (1) (pseudo)capacitance, associated with Li^+ adsorption on the TiO_2 surface; (2) diffusion-controlled intercalation of Li^+ into the TiO_2 lattice. The individual contributions of these two mechanisms were decoupled and analytically quantified. It has been ascertained that a remarkable 50% of the total charge was found to derive from a pseudocapacitive effect at 1 mV s^{-1}. Spectroelectrochemical investigations revealed a fast and reversible ion transport in charging/discharging processes, with an optical modulation of ~60% in the range of 315–1660 nm between the bleached and the colored state, and a coloration efficiency of 25.1 $cm^2\,C^{-1}$ at 550 nm. These results shown here establish that the overall lithium ion storage capabilities, as well as the electrochromic properties, directly benefit by reducing the size of TiO_2 particles to the nanodimensional range. The smaller size of the synthesised particles compared to commercial ones increases the pseudocapacitive contribution to the ions storage, resulting in a high contrast and fast switching kinetic at 550 nm and in a long-term stability of the electrode. Our results suggest that RP-TiO_2 shows great potential as a bifunctional material to work as an electrochromic smart windows and simultaneously to charge or power electronic devices, such as LEDs or sensors.

Acknowledgments

The authors gratefully aknowledge Progetto FISR—C.N.R. 'Tecnopolo di nanotecnologia e fotonica per la medicina di precisione'—CUP B83B17000010001, Apulia regional

project 'MOSAICOS—MOSAici Interattivi eCO-Sostenibili', Cod. HOQ3PM3—CUP B37H17004900007, Apulia regional project 'FONTANAPULIA—Fotocatalizzatori nanostrutturati e radiazione UV per un'acqua più pulita' Cod. WOBV6K5—CUP B37H17005230007 for funding.

R C Pullar thanks FCT (Fundação para a Ciência e Tecnologia, Portugal) Grant IF/00681/2015. This work was partly developed within the scope of the project CICECO-Aveiro Institute of Materials, UIDB/50011/2020 & UIDP/50011/2020, financed by national funds through the FCT/MEC and when appropriate co-financed by FEDER under the PT2020 Partnership Agreement. David Maria Tobaldi is overly grateful to FCT and to Portuguese national funds (OE), through FCT, I.P., in the scope of the framework contract foreseen in the numbers 4, 5 and 6 of the article 23, of the Decree-Law 57/2016, of August 29, changed by Law 57/2017, of July 19.

ORCID iDs

Roberto Giannuzzi https://orcid.org/0000-0002-0997-5686
Tania Prontera https://orcid.org/0000-0002-5934-7733
David M Tobaldi https://orcid.org/0000-0002-0112-8570
Marco Pugliese https://orcid.org/0000-0002-9502-8457
Luisa De Marco https://orcid.org/0000-0002-6855-5438
Robert C Pullar https://orcid.org/0000-0001-6844-4482

References

[1] Chen X and Mao S S 2007 *Chem. Rev.* **107** 2891
[2] Nakata K and Fujishima A 2012 *J. Photochem. Photobiol.* C **13** 169
[3] Oregan B and Gratzel M A 1991 *Nature* **353** 737
[4] Wu L, Bresser D, Buchholz D and Passerini S 2014 *J. Electrochem. Soc.* **162** A3052
[5] Karunagaran B, Uthirakumara P, Chunga S J, Velumani S and Suh E K 2007 *Mater. Charact.* **58** 680
[6] Ghicov A, Tsuchiya H, Hahn R, Macak J M, Munoz A G and Schmuki P 2006 *Electrochem. Commun.* **8** 528
[7] De Marco L, Manca M, Giannuzzi R, Belviso M R, Cozzoli P D and Gigli G 2013 *Energy Environ. Sci.* **6** 1791
[8] Singh J, Palsaniya S and Soni R K 2020 *Appl. Surf. Sci.* **527** 146796
[9] Mortimer R J, Rosseinsky D R and Monk P M S 2015 *Electrochromic Materials and Devices* (Weinheim: Wiley-VCH)
[10] Granqvist C G 1995 *Handbook of Inorganic Electrochromic Materials* (Amsterdam: Elsevier)
[11] Morgan B J and Watson G W 2010 *Phys. Rev.* B **82** 144119
[12] Anitha V C, Banerjee A N and Joo S W 2015 *J. Mater. Sci.* **50** 7495
[13] Dahlman C J, Tan Y, Marcus M A and Milliron D J 2015 *J. Am. Chem. Soc.* **137** 9160
[14] Nair P B, Justinvictor V B, Daniel G P, Joy K, Ramakrishnan V and Thomas P V 2011 *Appl. Surf. Sci.* **257** 10869
[15] Wang C M, Lin S Y and Chen Y C 2008 *J. Phys. Chem. Solids* **69** 451
[16] Yu J, Zhao X, Du J and Chen W 2000 *J. Sol-Gel Sci. Technol.* **17** 163
[17] Duyar O, Placido F and Durusoy H Z 2008 *J. Phys. D: Appl. Phys.* **41** 095307
[18] Brevet A, Fabreguette F, Imhoff L, Marco de Lucas M C, Heintz O, Saviot L, Sacilotti M and Bourgeois S 2002 *Surf. Coat. Technol.* **36** 151
[19] Wang J, Polleux J, Lim J and Dunn B 2007 *J. Phys. Chem.* C **111** 14925
[20] Augustyn V, Simon P and Dunn B 2014 *Energy Environ. Sci.* **7** 159è
[21] Patil S H, Gaikwad A P, Sathaye K R and Patil K R 2018 *Electrochim. Acta* **265** 556
[22] Kim C, Kim S, Lee J, Kim J and Yoon J 2015 *ACS Appl. Mater. Interfaces* **7** 7486
[23] Wang Q, Li M and Wang Z 2019 *RSC Adv.* **9** 7811
[24] Long B, Zhang J, Luo L, Ouyang G, Balogun M S, Song S and Tong Y 2019 *J. Mater. Chem.* A **7** 2626
[25] Li H, Lang J, Lei S, Chen J, Wang K, Liu L, Zhang T, Liu W and Yan X 2018 *Adv. Funct. Mater.* **28** 1800757
[26] Luo R, Ma Y, Qu W, Qian J, Li L, Wu F and Chen R 2020 *ACS Appl. Mater. Interfaces* **12** 23939
[27] Yang P H, Sun P, Chai Z S, Huang L H, Cai X, Tan S Z, Song J H and Mai W J 2014 *Angew. Chem. Int. Ed.* **53** 11935
[28] Martina F, Pugliese M, Serantoni M, Baldisserri C, Gorni G, Maggiore A, Gigli G and Maiorano V 2017 *Sol. Energy Mater. Sol. Cells* **160** 435
[29] Cossari P, Pugliese M, Gambino S, Cannavale A, Maiorano V, Gigli G and Mazzeo M 2018 *J. Mater. Chem.* **6** 7274
[30] Tobaldi D M, Rozman N, Leoni M, Seabra M P, Skapin A S, Pullar R C and Labrincha J A 2015 *J. Phys. Chem.* C 2015 **119** 23658
[31] Tobaldi D M, Pullar R C, Gualtieri A F, Seabra M P and Labrincha J A 2013 *Chem. Eng. J.* **214** 364
[32] Ito S, Chen P, Comte P, Nazzeruddin M K, Liska P, Pechy P and Gratzel M 2007 *Prog. Photovolt.* **15** 603
[33] De Marco L, Manca M, Giannuzzi R, Malara F, Melcarne G, Ciccarella G, Zama I, Cingolani R and Gigli G 2010 *J. Phys. Chem.* C **114** 4228
[34] Giannuzzi R, De Donato F, De Trizio L, Monteduro A G, Maruccio G, Scarfiello R, Qualtieri A and Manna L 2019 *ACS Appl. Mater. Interfaces* **11** 39921
[35] Tobaldi D M, Pullar R C, Seabra M P and Labrincha J A 2014 *Mater. Lett.* **122** 345
[36] Supriynato A, Nandani, Wahyuningsih S and Ramelan A H 2018 *IOP Conf. Ser.: Mater. Sci. Eng.* **333** 012028
[37] Lindstrom H, Sodergren S, Solbrand A, Rensmo H, Hjelm J, Hagfeldt A and Lindquist S E 1997 *J. Phys. Chem.* B **101** 7710
[38] Lindstrom H, Sodergren S, Solbrand A, Rensmo H, Hjelm J, Hagfeldt A and Lindquist S E 1997 *J. Phys. Chem.* B **101** 7717
[39] Wang Q, Wen Z H and Li J H 2006 *Inorg. Chem.* **45** 6944
[40] Moitzheim S, De Gendt S and Vereecken P M 2019 *J. Electrochem. Soc.* **166** A1
[41] Van de Krol R, Goossens A and Schoonman J 1999 *J. Phys. Chem.* B **103** 7151
[42] Brezesinski T, Wang J, Polleux J, Dunn B and Tolbert S H 2009 *J. Am. Chem. Soc.* **131** 1802
[43] Ardizzone S, Fregonara G and Trasatti S 1989 *Electrochim. Acta* **35** 263
[44] Liu Y, Zhang N, Jiao L and Chen J 2015 *Adv. Mater.* **27** 6702
[45] Hou H, Banks C E, Jing M, Zhang Y and Ji X 2015 *Adv. Mater.* **27** 7861
[46] Zhang C *et al* 2016 *Nano Lett.* **16** 2054
[47] Liu Z, Yu X-Y, Lou X W and Paik U 2016 *Energy Environ. Sci.* **9** 2314
[48] Gogotsi Y and Simon P 2011 *Science* **334** 917

[49] Dhandayuthapani T, Sivakumar R, Ilangovan R, Gopalakrishnan C, Sanjeeviraja C, Sivanantharaja A, Hari and Krishna R 2018 *J. Solid State Electrochem.* **460** 1825
[50] Dinh N N, Oanh N T T, Long P D, Bernard M C, Hugot-Le and Goff A 2003 *Thin Solid Films* **423** 70
[51] Meher S R and Balakrishnan L 2014 *Mater. Sci. Semicond. Process.* **26** 251
[52] Verma A, Basu A, Bakhshi A K and Agnihotry S A 2005 *Solid State Ion.* **176** 2285
[53] Nang Dinh N, Minh Quyen N, Chung D N, Zikova M and Truong V V 2011 *Sol. Energy Mater. Sol. Cells* **95** 618
[54] Chen J Z, Ko W Y, Yen Y C, Chen P H and Lin K J 2012 *ACS Nano* **6** 6633
[55] Liu S, Zhang X, Sun P, Wang C, Wei Y and Liu Y 2014 *J. Mater. Chem.* C **2** 7891
[56] Şilik E, Pat S, Özen S, Mohammadigharehbagh R, Yudar H H, Musaoğlu C and Korkmaz Ş 2017 *Thin Solid Films* **640** 27
[57] Akkurt N, Pat S, Mohammadigharehbagh R, Özgür M, Demirkol U, Olkun A and Korkmaz Ş 2020 *J. Mater. Sci. Mater. Electron.* **31** 9568
[58] Khalifa Z S 2014 *Sol. Energy Mater. Sol. Cells* **124** 186
[59] Lee K, Kim D, Berger S, Kirchgeorg R and Schmuki P 2012 *J. Mater. Chem.* **22** 9821
[60] Triana C A, Granqvist C G and Niklasson G A 2014 *J. Phys.: Conf. Ser.* **559** 1